Atmospheric-pressure dielectric barrier discharge cold plasma for synthesizing high performance Pd/C formic acid dehydrogenation catalyst

Lanbo Di[1]*, Jingsen Zhang[1], Cunhua Ma[2], Xin Tu[3], Xiuling Zhang[1]*

[1] College of Physical Science and Technology, Dalian University, Dalian 116622, China

[2] School of Chemistry and Chemical Engineering, Shihezi University, Shihezi 832003, China

[3] Department of Electrical Engineering and Electronics, University of Liverpool, Liverpool L69 3GJ, U.K.

---

* Corresponding authors.

E-mail addresses: dilanbo@163.com (L.B. Di), xiulz@sina.com (X.L. Zhang).

HCOOH is a cheap, non-toxic, ease of storage and transportation, and abundant renewable source for generating hydrogen. Activated carbon supported palladium (Pd/C) catalysts have drawn increasing research interest due to their high performance toward HCOOH dehydrogenation and ease of recycle after deactivation. In this work, atmospheric-pressure (AP) dielectric barrier discharge (DBD) cold plasma has been employed to synthesize Pd/C-P catalyst by using $PdCl_2$ as Pd precursor. For comparison, commercial Sigma-Aldrich Pd/C catalyst is adopted as the reference. Both cold plasma synthesized Pd/C-P and commercial Pd/C catalysts exhibit high performance for HCOOH dehydrogenation, and no CO is detected. The total volume of generated H_2 and CO_2 over Pd/C-P is 317 ml, which is 1.12 times as that of commercial Pd/C (282 ml). The catalytic stability of Pd/C-P is much superior to the commercial Pd/C catalyst. Catalytic activity of Pd/C-P has been decreased to 59.6% and 50.2% after the second and third reaction cycle, respectively, in comparison with the first cycle. However, they have been decreased to 16.3% and 8.9%, respectively, for commercial Pd/C. Various characterization techniques have been adopted to discuss the influence mechanism. The high catalytic activity of Pd/C-P is mainly attributed to the small size of Pd nanoparticles. The high catalytic stability of Pd/C-P is ascribed to the strong metal-support interaction induced by cold plasma and HNO_3 pre-oxidation treatment, which leads to less decrease in Pd/C atomic ratio, Pd leaching, and stabilizes the size of Pd nanoparticles. In conclusion, the Pd/C-P catalyst exhibits much higher catalytic activity and stability than the commercial Pd/C, which has theoretical significance and practical application value.

Keywords: atmospheric-pressure cold plasma; dielectric barrier discharge (DBD); Pd/C; formic acid dehydrogenation; supported metal catalysts

1. Introduction

With the exhaustion of fossil fuels and the resulting environmental deterioration problems, the development and usage of clean energy has become an urgent problem to be solved. Hydrogen (H_2) is an important clean and renewable energy source, and it is a perfect candidate to meet the world's energy demand without toxic emissions [1]. However, widespread utilization of hydrogen gas is confined to its capacity limitations of storage, as well as the safety issues concerned with the storage and transportation under mild conditions [2]. Therefore, how to produce hydrogen from cheap and abundant renewable sources is a key scientific problem for using hydrogen as energy carrier. Biomass, ammonia borane and formic acid (HCOOH) have been extensively investigated as the potential candidates for hydrogen storage [3-6]. Among them, HCOOH is superior due to its non-toxicity, abundance and easy storage and transportation. In addition, hydrogen generation reaction can be carried out at ambient temperature [7-8], which renders HCOOH attractive for portable fuel cells applications as the hydrogen carrier.

There are two pathways for HCOOH decomposition: dehydrogenation and dehydration. Hydrogen generation can be achieved by HCOOH dehydrogenation according to equation (1), which is a popular reaction process. In addition, an undesirable dehydration pathway equation (2) should be avoided for two reasons. On the one hand, hydrogen can not be effectively

generated from equation (2). On the other hand, CO will be formed during HCOOH dehydration, which is toxic to the fuel cell catalysts [9]. Various catalysts have been developed to avoid the HCOOH dehydration way, and Pd/C catalysts have drawn increasing research interest due to their high performance for HCOOH dehydrogenation and ease of recycle after deactivation [10-12]. Moreover, commercial Pd/C catalysts produced by Sigma-Aldrich are often adopted as the reference to compare the catalysts for HCOOH dehydrogenation.

$$\text{Dehydrogenation: } HCOOH(l) = H_2(g) + CO_2(g) \quad \Delta G_{298K} = -35.0 \text{ kJ·mol}^{-1} \tag{1}$$

$$\text{Dehydration: } HCOOH(l) = H_2O(l) + CO(g) \quad \Delta G_{298K} = -14.9 \text{ kJ·mol}^{-1} \tag{2}$$

Since HCOOH dehydrogenation is carried out in liquid phase, the aggregation and leaching of the Pd nanoparticles are two important factors influencing the catalytic activity and stability of the Pd/C catalysts, which are vital for practical applications. Synthesizing Pd/C catalysts with small size and high dispersion of Pd nanoparticles, as well as strong metal-support interaction are efficient for solving this problem.

Cold plasma is non-equilibrium plasma. The electron temperature in it can be above 10,000 K, while the gas temperature can be close to room temperature. Cold plasma has been proved to be an efficient method for synthesizing high performance supported metal catalysts, and has attracted great research attentions [13-16]. By tuning the working parameters of cold plasma, supported metal catalysts with small size and high dispersion of metal nanoparticles, as well as enhanced metal-support interaction can be obtained. In addition, the crystallinity, crystal face, and alloying degree of the supported metal catalysts can also be adjusted by cold plasma preparation [17-24]. For example, Liang et al. [25] adopted argon glow discharge

plasma to synthesize Pd/Al_2O_3 catalysts for selective oxidation of glucose to gluconic acid. The plasma synthesized catalyst exhibited higher activity than conventional method, and it showed high stability against leaching of the active metal into the reaction medium. Di et al. [26] used AP DBD cold plasma to synthesize Pt/TiO_2 catalyst, and the catalyst showed high dispersion and smaller size of Pt particles, and enhanced metal-support interaction. Hong et al. [27] used glow discharge plasma for preparing Co/TiO_2 Fischer-Tropsch synthesis catalysts promoted by Pt. The cobalt particle size can be effectively tuned by changing plasma treatment duration. $CoPt/TiO_2$ catalyst with homogeneously and highly dispersed cobalt nanoparticles (~1 nm) was achieved, and plasma not only increased the amount of active sites, but also enhanced the specific reactivity.

In this work, a simple AP DBD cold plasma was adopted to synthesize Pd/C catalyst toward HCOOH dehydrogenation reaction. The cold plasma synthesized Pd/C-P catalyst showed much higher catalytic activity and stability for HCOOH dehydrogenation than the commercial Pd/C catalyst. Various characterization techniques are adopted to analyze the structure of the Pd/C catalysts, and the influence mechanism has been disclosed.

2. Experimental

2.1. Materials

Palladium chloride ($PdCl_2$) was obtained from Tianjin Kemiou Chemical Reagent Co., Ltd, China. Formic acid (HCOOH, ≥96%), sodium formate (HCOONa, ≥96%) and commercial Pd/C (5.0wt% of Pd) were purchased from Sigma-Aldrich. Activated carbon with specific surface area of 852.0 $m^2 \cdot g^{-1}$ was supplied by Beijing Guanghua Timber Mill.

2.2. Catalyst preparation

Prior to preparing the Pd/C catalysts, the activated carbon was crushed and sieved to 40-60 mesh size, and pre-oxidized by nitric acid (HNO_3) according to a previous literature [28]. Briefly, 3 g of activated carbon was added into 15 ml of 30wt% HNO_3. Then, the mixture was kept at 85 ^oC for 5 h, washed by deionized water until the pH of the solution reached ca. 7. Finally, the obtained activated carbon was dried at 120 ^oC for 2 h to be investigated.

The Pd precursor was supported on activated carbon by a simple incipient wetness impregnation method, and the loading amount of metal Pd was 5.0wt%. The activated carbon supported $PdCl_2$ was calcined at 300 ^oC for 2 h under hydrogen atmosphere with a heating rate of 5 $^oC \cdot min^{-1}$. Then the obtained sample was treated by AP plate-to-plate DBD cold plasma, and the obtained catalyst was denoted as Pd/C-P. For comparison, commercial Pd/C catalyst with same Pd loading amount (5.0wt% of Pd) was purchased from Sigma-Aldrich and marked as Pd/C.

Detailed description of the AP plate-to-plate DBD cold plasma device can be found in our previous work [29]. A sinusoidal CTP-2000K power supply (Nanjing Suman Electronic Co. Ltd.) was employed to ignite the AP DBD cold plasma. The peak-to-peak discharge voltage ($U_{p\text{-}p}$) and discharge frequency (f) were kept at 36.0 kV and 13.6 kHz, respectively. High purity hydrogen gas (>99.999%) with 100 $ml \cdot min^{-1}$ flow rate was adopted as the working gas. 0.5 g sample was uniformly distributed in the DBD quartz reactor. The treatment was conducted for 3 times (2 min for each treatment). The sample was manually stirred between two operations to achieve uniform treatment.

2.3. Catalytic tests of HCOOH dehydrogenation

To analyze the catalytic performance of the samples, catalytic activity and stability of HCOOH dehydrogenation over the Pd/C catalysts were tested. 50 mg of Pd/C sample and 10 ml of deionized water were mixed in a rubber plug sealed distillation flask, and heated in a thermostat water bath at 50 ^{o}C with a 200 r·min^{-1} magnetic stirring. Then, 2 ml of HCOOH (4 mol·L^{-1}) and 8 ml of HCOONa (4 mol·L^{-1}) were injected into the flask. The HCOOH dehydrogenation reaction using the Pd/C catalysts was performed at 50 ^{o}C. The generated hydrogen (H_2) and carbon dioxide (CO_2) gases were monitored by a GC7890 gas chromatography (Tianmei Scientific instrument Co. Ltd., China) with a TCD detector using carbon molecular sieve (TDX-01) column. No carbon monoxide (CO) was detected during the reaction. The volume of the H_2 and CO_2 was measured by an inverted measuring cylinder at 25 ^{o}C. After testing the catalytic activity, the Pd/C catalysts were separated by filtering, and washed by deionized water for 3 times to remove the residual HCOOH and HCOONa. Then the recycled Pd/C catalysts were dried at 110 ^{o}C for 2 h to be investigated for the second and third reaction cycle to test their catalytic stability.

2.4. Catalyst characterization

X-ray diffraction (XRD) patterns of the samples were measured by a DX-2700 (Dandong Haoyuan Instrument Co. Ltd., China) X-ray diffractometer operating at 40 kV and 30 mA using Cu K_α radiation (λ = 0.154178 nm). To investigate the microscopy of the samples, a HT7700 transmission electron microscope (Hitachi, Japan) operating at 120 kV accelerating voltage was employed. The average size of the Pd nanoparticles was obtained by measuring more than 100 nanoparticles. X-ray photoelectron spectroscopy (XPS, ESCALAN250, Thermo VG) with a monochromatized Al K_α (1486.6 eV) X-ray source was used to

investigate the chemical composition and binding states of the catalysts. All binding energies were calibrated according to the C1s peak of graphitic carbon at 284.6 eV. A NOVA2200e gas sorption analyzer (Quantachrome Corp., USA) was adopted to measure the pore volumes (V_p), pore sizes (D_p), and the Brunauer-Emmett-Teller (BET) specific surface areas (S_{BET}) of the samples by nitrogen adsorption/desorption. The samples were dried at 110 ^oC for 2 h, and outgassed at 200 ^oC for 5 h prior to adsorption analysis. Barrett–Joyner–Halenda (BJH) model with the Halsey equation was used to analyze the adsorption and desorption data. The concentrations of Pd in the Pd/C samples before and after HCOOH dehydrogenation reaction were determined by inductively coupled plasma optical emission spectroscopy (ICP-OES, Varian 720-ES).

3. Results and discussion

3.1 Catalytic activity and stability of the Pd/C catalysts

Figure 1 presents the HCOOH dehydrogenation catalytic activity of the Pd/C-P synthesized by cold plasma and the commercial Pd/C purchased from Sigma-Aldrich. Both of the Pd/C catalysts exhibit high HCOOH dehydrogenation catalytic activity. The total volume of generated H_2 and CO_2 over Pd/C-P is 317 ml, which is 1.12 times as that of commercial Pd/C (282 ml). Accordingly, the decomposition rate of HCOOH over Pd/C-P has reached 81.1% after 230 min reaction time. However, the initial catalytic activity of commercial Pd/C is much higher than Pd/C-P. The largest volume of generated H_2 and CO_2 over commercial Pd/C is obtained after ca. 110 min reaction time. In contrast, a slow gas generation rate is observed for Pd/C-P, and the total volume of generated H_2 and CO_2 is increasing until after 230 min.

To further investigate the performance of the Pd/C catalysts, HCOOH dehydrogenation catalytic stability of the Pd/C-P and commercial Pd/C is also investigated. The plots of generated H_2 and CO_2 gas volume versus time over the Pd/C catalysts for three cycles are illustrated in Figure 2. The total volumes of generated H_2 and CO_2 over the cold plasma synthesized Pd/C-P catalyst for three cycles are 317, 189, 159 ml, respectively. Whereas, they are 282, 46, 25 ml, respectively, for the commercial Pd/C catalyst. Obviously, deactivation is observed for both of the Pd/C catalysts. The catalytic activity (the generated total gas volume) over Pd/C-P has been decreased to 59.6% and 50.2% after two and three reaction cycles, respectively, in comparison with the first cycle. However, they have been decreased to 16.3% and 8.9%, respectively for commercial Pd/C. Interestingly, catalytic activity of Pd/C-P-3R is 6.36 times as that of commercial Pd/C-3R after three reaction cycles. This indicates that commercial Pd/C catalyst is more prone to deactivation than cold plasma synthesized Pd/C-P catalyst. In other words, Pd/C-P shows much higher catalytic stability. To get insight into the intrinsic influence mechanism of the catalytic activity and stability of the Pd/C catalysts, XRD, TEM, XPS and BET characterizations were performed to investigate the structure of the catalysts, and the structure-performance relationship of the Pd/C catalysts are discussed.

3.2 Characterization of the Pd/C catalysts

As shown in Figure 3, XRD patterns of Pd/C-P and Pd/C before and after HCOOH dehydrogenation test are measured to investigate the crystal structure of the catalysts. From the XRD pattern of Pd/C-P, it can be seen that no obvious metallic Pd characteristic peaks (JCPDS card, file no. 46-1043) [30] or other Pd species can be detected. Meantime, after two and three reaction cycles, no obvious change can be found for the XRD patterns. These

suggest that the Pd nanoparticles in cold plasma synthesized Pd/C-P catalyst have small size and are highly distributed on the activated carbon support. In addition, the HCOOH dehydrogenation reaction in liquid phase does not result in the aggregation of the Pd nanoparticles. However, from the XRD pattern of the as-purchased commercial Pd/C catalyst, we can see that weak diffraction peaks at 40.1^{o} and 46.6^{o}, corresponding to the (111) and (200) planes of the face centered cubic structure of metallic Pd are observed. This reveals that the size of the Pd nanoparticles in commercial Pd/C is larger than that in Pd/C-P synthesized by cold plasma. Different from the change trend of the XRD patterns for Pd/C-P, the intensity of the characteristic peaks of metallic Pd for commercial Pd/C is enhanced after HCOOH dehydrogenation test, suggesting that aggregation of Pd nanoparticles appeared due to the liquid reaction. Compared with the commercial Pd/C catalyst, the small size of Pd nanoparticles for Pd/C-P before and after HCOOH dehydrogenation test is attributed to the enhanced metal-support interaction. This phenomenon has been observed in previous work [25].

To further investigate the size and size distribution of the Pd nanoparticles in the Pd/C catalysts, TEM images of Pd/C-P and commercial Pd/C catalysts before and after three reaction cycles are obtained, as shown in Figure 4. From the TEM images, we can see that all Pd nanoparticles in the Pd/C-P catalysts as-synthesized and after three reaction cycles are highly distributed on the activated carbon support. In contrast, weak aggregation of the Pd nanoparticles is observed for the commercial Pd/C catalysts as-purchased and after three reaction cycles. As illustrated in Figure 4, histograms of size distribution of Pd nanoparticles are also obtained by measuring more than 100 Pd nanoparticles, and the data are summarized

in Table 1. The average size of Pd nanoparticles (D_{mean}) for the as-synthesized Pd/C-P is 2.7±1.1 nm, which is smaller than that for commercial Pd/C (3.3±1.1 nm). Interestingly, D_{mean} for Pd/C-P-3R is 2.7±0.8 nm, which is similar with that for the as-synthesized Pd/C-P catalyst. This further confirms the enhanced metal-support interaction in Pd/C-P catalyst synthesized by cold plasma. In contrast, D_{mean} for Pd/C-3R is 4.0±1.1 nm, which is larger than that for the as-purchased commercial Pd/C catalyst. These phenomena are in line with the XRD results (Figure 3), and they further confirm the small size of the Pd nanoparticles and the enhanced metal-support interaction in Pd/C-P.

The Pd3d core levels on the surface of Pd/C-P and commercial Pd/C catalysts before and after three reaction cycles were measured by XPS to investigate the composition of the Pd species, as shown in Figure 5. Pd3d XPS spectra for the four samples can be deconvoluted into three peaks at 335.9, 337.8, 338.3 eV, ascribing to Pd^0, Pd^{II} and Pd^{IV}, respectively [28]. The compositions of the Pd species are obtained according to the Pd3d XPS spectra, as summarized in Table 1. The Pd precursor in the Pd/C samples was not completely reduced into metallic Pd due to the abundant oxygen species on the activated carbon surface, which was also observed in previous work [28,31]. The ratios of metallic Pd in cold plasma synthesized Pd/C-P and commercial Pd/C are 66.0% and 55.4%, respectively. The high ratio of metallic Pd for Pd/C-P is attributed to the combination of cold plasma reduction and thermal reduction. In this work, hydrogen gas was used as the working gas to generate active hydrogen species to reduce the Pd precursor to synthesize metallic Pd nanoparticles. The active hydrogen species, including ground-state hydrogen atoms (H) and excited-state hydrogen atoms (H*) and molecules (H_2*), can not only reduce metallic ions with positive

standard potentials but also some with negative values [13-14]. The ratio of metallic Pd in Pd/C-P-3R is decreased from 66.0% (for the as-synthesized Pd/C-P) to 53.1% after three reaction cycles. However, no obvious change is detected for the commercial Pd/C as-purchased and after three reaction cycles.

According to the Pd3d and C1s XPS spectra, the Pd/C atomic ratios of the Pd/C catalysts before and after 3 reaction cycles are also obtained, as illustrated in Table 1. There is no obvious difference in the Pd/C atomic ratio, and they are 0.0140 and 0.0147, respectively, for Pd/C-P and commercial Pd/C. In spite of this, they were decreased to 0.0125 and 0.0087 for Pd/C-P-3R and Pd/C-3R after three reaction cycles. The Pd/C atomic ratio for Pd/C-P-3R is decreased only by 10.7% after three reaction cycles. However, significant decrease (40.8%) in Pd/C atomic ratio for the Pd/C-3R after three reaction cycles is observed. The less decrease in Pd/C atomic ratio for the cold plasma synthesized Pd/C-P-3R catalyst can be attributed to the strong metal-support interaction by cold plasma. It has been confirmed by the results of XRD patterns (Figure 3) and TEM images (Figure 4). In other words, the cold plasma synthesized Pd/C-P catalyst shows higher stability than the commercial Pd/C catalyst.

Multilayer physisorption of N_2 were performed to investigate the porous structure of the Pd/C catalysts. Nitrogen adsorption-desorption isotherms of the cold plasma synthesized Pd/C-P and commercial Pd/C catalysts before and after HCOOH dehydrogenation test, and the corresponding pore size distribution curves are illustrated in figure 6. As shown in figure 6a, at low relative pressure (p/p_0 = 0-0.40), a rapid increase of adsorption amount is observed for the commercial Pd/C catalysts before and after activity test due to the occupation of the microporous pores, which is the characteristic behavior of type I isotherm according to the

IUPAC classification. In addition, type IV isotherm with a type H3 hysteresis loop appears at a relative pressure of 0.4-0.99, revealing their mesoporous structure with slit-shaped pores [32]. The adsorption at the medium pressure (p/p_0 = 0.40-0.85) for the samples is mainly ascribed to capillary condensation of N_2 in mesopores. The rapid increase of adsorption amount at the medium pressure indicates that there is a wide distribution of the mesopores for commercial Pd/C, which is consistent with the results of the pore size distributions presented in Figure 6c. In addition, the adsorption at the high pressure (p/p_0 = 0.85-0.99) is attributed to the aggregation in pores. Therefore, commercial Pd/C catalysts are the mixture of microstructure and mesoporous structure [33], which are also confirmed by the wide pore size distribution (0-100 nm) in Figure 6c. From figure 6b, type IV isotherm with a type H4 hysteresis loop at a relative pressure of 0.4-0.99 [34] is observed for the cold plasma synthesized Pd/C-P catalysts. Different from the commercial Pd/C catalysts, weak increase of adsorption amount at the medium pressure is detected, suggesting that there is a narrow pore size distribution in Pd/C-P catalysts. This is consistent with the results of pore size distribution (3-8 nm) for the Pd/C-P catalysts in figure 6d.

The pore volumes (V_p), pore sizes (D_p), and the Brunauer-Emmett-Teller (BET) specific surface areas (S_{BET}) of the samples were summarized in Table 2. The S_{BET} of the as-purchased commercial Pd/C is 913.7 $m^2 \cdot g^{-1}$, which is 1.11 time as that of the as-synthesized Pd/C-P catalyst (822.2 $m^2 \cdot g^{-1}$). Obvious decrease in S_{BET} is observed for both the Pd/C-P and commercial Pd/C catalysts after HCOOH dehydrogenation test. The S_{BET} for Pd/C-3R has been decreased from 913.7 to 635.5 $m^2 \cdot g^{-1}$ after three reaction cycles, and it is about 69.6% as that of the as-purchased commercial Pd/C catalyst. In contrast, less decrease in the S_{BET} is

observed for the cold plasma synthesized Pd/C-P catalyst after three reaction cycles, and it is 75.4% as that of the as-synthesized Pd/C-P. Additionally, the commercial Pd/C catalyst has larger pore size volume (0.444 $cm^3 \cdot g^{-1}$) than Pd/C-P (0.007 $cm^3 \cdot g^{-1}$). A significant decrease in V_p is detected for the commercial Pd/C catalyst after three reaction cycles. However, an increase in V_p is detected for Pd/C-P, which may be induced by the acid reaction environmental. In brief, the BET data also indicate that the Pd/C-P shows higher stability than the commercial Pd/C catalysts.

The concentrations of Pd in the Pd/C samples before and after HCOOH dehydrogenation reaction were determined by ICP experiments, and the data are also summarized in Table 2. The actual Pd loading amount in commercial Pd/C and cold plasma synthesized Pd/C-P are 5.10% and 5.02%, respectively. The Pd loading amount of Pd/C-3R after three reaction cycles is 87.8% as that of the as-purchased Pd/C, while it is 92.6% as that of the as-synthesized Pd/C-P for Pd/C-P-3R. This can be attributed to the strong metal-support interaction caused by cold plasma preparation [25, 26] and the abundant oxygen-containing groups on the activated carbon support formed by HNO_3 pre-oxidation, which further confirms the stability of the cold plasma synthesized Pd/C-P catalyst. Enhanced metal-support interaction for the supported metal catalysts synthesized by cold plasma had been observed in previous work [35,36], and it was attributed to the electric field distribution in cold plasma, and the plasma parameters, such as the power coupling with the plasma, the gas pressure, the chemical composition of the plasma, etc. [37]. Future work will be carried out to further enhance the metal-support interaction in the Pd/C-P catalyst by tuning the plasma parameters.

3.3 Discussion

The cold plasma synthesized Pd/C-P catalyst exhibits higher catalytic activity for HCOOH dehydrogenation, and the total volume of generated H_2 and CO_2 over Pd/C-P is 1.12 times as that over commercial Pd/C. However, the commercial Pd/C catalyst shows higher initial reaction rate (Figure 1) than Pd/C-P. The reaction time to achieve the largest volume of generated H_2 and CO_2 over commercial Pd/C is ca. 110 min, while it is ca. 230 min for Pd/C-P. Hu et al. [38] found that the size of Pd nanoparticles play important roles in HCOOH dehydrogenation reaction. The optimal size of Pd nanoparticles should be in the range of 1.8-3.5 nm, and smaller or larger size of Pd nanoparticles on carbon support had negative effect on HCOOH dehydrogenation. The XRD patterns of the Pd/C catalysts (Figure 3) indicate that the Pd diffraction peaks can not be detected for cold plasma synthesized Pd/C-P, while weak characteristic peaks corresponding to metallic Pd can be detected for commercial Pd/C. Correspondingly, the result of TEM images indicates that the sizes of Pd nanoparticles in Pd/C-P and Pd/C are 2.7±1.1 nm and 3.3±1.1 nm, respectively. Meantime, they are 2.7±0.9 nm and 4.0±1.1 nm, respectively in Pd/C-P-3R and Pd/C-3R after three reaction cycles. These reveal that the size of Pd nanoparticles in commercial Pd/C catalyst is not as stable as that in plasma synthesized Pd/C-P. Therefore, the high catalytic activity of Pd/C-P is mainly attributed to the smaller size and higher stability of Pd nanoparticles. The higher initial activity of commercial Pd/C is mainly attributed to its higher specific surface and larger pore volume (Table 2).

Figure 2 shows that the cold plasma synthesized Pd/C-P catalyst exhibits higher catalytic stability toward HCOOH dehydrogenation than the commercial Pd/C. Deactivation phenomenon was observed for both Pd/C-P and Pd/C during HCOOH dehydrogenation test.

The generated total gas volume over Pd/C-P has been decreased to 59.6% and 50.2%, respectively, as that for the first cycle, while they have been decreased to 16.3% and 8.9%, respectively, for commercial Pd/C. The catalytic activity of the Pd/C catalysts is closely related with the specific surface area of the catalysts, the Pd/C atomic ratio, the actual Pd loading amount, as well as the size of the Pd nanoparticles. Therefore, the decrease of the catalytic activity after three reaction cycles can be analyzed as follows. Firstly, the S_{BET} for Pd/C-3R has been decreased to 69.6% as that of the as-purchased commercial Pd/C catalyst, while the S_{BET} for Pd/C-P-3R is75.4% as that of the as-synthesized Pd/C-P. Secondly, the Pd/C atomic ratio for Pd/C-3R after three reaction cycles obtained from the XPS data has been decreased from 0.0147 to 0.0087, corresponding to a 40.8% decrease. In contrast, the Pd/C atomic ratio for Pd/C-P-3R has been decreased from 0.0140 to 0.0125 after three reaction cycles, corresponding to a 10.7% decrease. Moreover, the actual Pd loading amount for Pd/C-3R and Pd/C-P-3R have been decreased to 87.8% and 92.6%, respectively, as that of the as-obtained Pd/C catalysts. From what have been discussed above, it can be seen that less decrease in the specific surface area, Pd/C atomic ratio and Pd leaching can be observed for the cold plasma synthesized Pd/C-P than the commercial Pd/C catalyst. At last, the fast deactivation of the commercial Pd/C catalyst can also be attributed to the aggregation of the Pd nanoparticles. The size of the Pd nanoparticles for Pd/C-3R has been increased from 3.3±1.1 to 4.0±1.1 nm after three reaction cycles. Hu et al. [38] claimed that the Pd/C with particle sizes larger than 4 nm showed poor activity toward HCOOH dehydrogenation. However, no obvious size change can be observed for the cold

plasma synthesized Pd/C-P catalysts even after three reaction cycles. The less decrease in the Pd/C atomic ratio and Pd leaching, as well as the stable size of Pd nanoparticles for Pd/C-P can be attributed to the strong metal-support interaction induced by cold plasma and the abundant oxygen-containing groups on the activated carbon support formed by HNO_3 pre-oxidation [28]. In conclusion, the Pd/C-P catalyst exhibits much higher catalytic activity and stability than the commercial Pd/C.

4. Conclusion

In this work, a simple AP DBD cold plasma has been employed to synthesize Pd/C-P catalyst by using $PdCl_2$ as Pd precursor for HCOOH dehydrogenation application. For comparison, commercial Sigma-Aldrich Pd/C catalyst is adopted as the reference. Both cold plasma synthesized Pd/C-P and commercial Pd/C catalysts exhibit high performance for HCOOH dehydrogenation, and no CO is detected. The cold plasma synthesized Pd/C-P shows higher catalytic activity and stability than the commercial Pd/C catalyst. The total volume of generated H_2 and CO_2 over Pd/C-P is 1.12 times as that of commercial Pd/C. Catalytic activity of Pd/C-P has been decreased to 59.6% and 50.2% after second and third cycle, respectively, in comparison with the first cycle. However, they have been decreased to 16.3% and 8.9%, respectively, for commercial Pd/C. The high catalytic activity of Pd/C-P is mainly attributed to the small size of Pd nanoparticles. The high catalytic stability of Pd/C-P is ascribed to the strong metal-support interaction induced by cold plasma and HNO_3 pre-oxidation treatment, which lead to the less decrease in the Pd/C atomic ratio, Pd leaching, and the stable size of Pd nanoparticles. AP DBD cold plasma method is an efficient method

for synthesizing high catalytic activity and stability Pd/C catalysts, which has theoretical significance and practical application value.

Acknowledgements

This work is supported by National Natural Science Foundation of China (Grant No. 21773020, 21673026, 11505019), the Liaoning Innovative Talents in University (Grant No. LR2017025), and the Natural Science Foundation of Liaoning Province (Grant No. 20180550085).

References

[1] S.E. Hosseini, M.A. Wahid, Renew. Sust. Energ. Rev. 57 (2016) 850.

[2] S.Z. Baykara, Int. J. Hydrogen Energ. 30 (2005) 545.

[3] X.Q. Du, C.L. Yang, X. Zeng, T. Wu, Y.H. Zhou, P. Cai, G.Z. Cheng, W. Luo, Int. J. Hydrogen Energ. 42 (2017) 14181.

[4] P. Sivagurunathan, G. Kumar, A. Mudhoo, Renew. Sust. Energ. Rev. 77 (2017) 28.

[5] Z. Li, Q. Xu, Accounts chem. Res. 50 (2017) 1449.

[6] S. Akbayrak, Y. Tonbul, S. Özkar, Appl. Catal. B-Environ. 206 (2017) 384.

[7] P.L. Liu, X.J. Gu, H. Zhang, J. Cheng, J. Song, H.Q. Su, Appl. Catal. B-Environ. 204 (2017) 497.

[8] K. Jiang, K. Xu, S.Z. Zou, W.B. Cai, J. Am. Chem. Soc. 136 (2014) 4861.

[9] M. Yadav, T. Akita, N. Tsumori, Q. Xu, J. Mater. Chem. 22 (2012) 12582.

[10] F. Sanchez, D. Motta, A. Roldan, C. Hammond, A. Villa, N. Dimitratos, Top. Catal. 61 (2018) 254.

[11] H. Jeon, Y.M. Chung, Appl. Catal. B-Environ. 210 (2017) 212.

[12] M. Zacharska, L.G. Bulusheva, A.S. Lisitsyn, S. Beloshapkin, Y.N. Guo, E.V. Shlyakhova, O.Y. Podyacheva, J.J. Leahy, A.V. Okotrub, D.A. Bulushev, ChemSusChem 10 (2017) 720.

[13] L.B. Di, J.S. Zhang, X.L. Zhang, Plasma Processes Polym. 15 (2018) 1700234.

[14] Z. Li, L.B. Di, F. Yu, X.L. Zhang, Acta Phys. Sin-Ch Ed 67 (2018) 215202.

[15] Z. Wang, Y. Zhang, E.C. Neyts, X.X. Cao, X.S. Zhang, B.W.L. Jang, C.J. Liu, ACS Catal. 8 (2018) 2093.

[16] W. Chu, J.Q. Xu, J.P. Hong, T. Lin, A. Khodakov, Catal. Today 256 (2015) 41.

[17] Q.C. Tran, H. An, H. Ha, V.T. Nguyen, N.D. Quang, H.Y. Kim, H.S. Choi, J. Mater. Chem. A 6 (2018) 8259.

[18] S. Zhang, X.S. Li, B. Zhu, J.L. Liu, X. Zhu, A.M. Zhu, B.W.L. Jang, Catal. Today 256 (2015) 142.

[19] J. Wang, S. Kattel, Z. Wang, J.G. Chen, C.J. Liu, ACS Appl. Mater. Inter. 10 (2018) 21321.

[20] L.B. Di, Z. Li, B. Lee, D.W. Park, Int. J. Hydrogen Energ. 42 (2017) 11372.

[21] L. Wang, Y. Yi, H. Guo, X. Tu, ACS Catal. 8 (2018) 90.

[22] L.B. Di, D.Z. Duan, D.W. Park, W.S. Ahn, B.J. Lee, X.L. Zhang, Top. Catal. 60 (2017) 925.

[23] Z.J. Xu, B. Qi, L.B. Di, X.L. Zhang, J. Energ. Chem. 23 (2014) 679.

[24] W.J. Xu, Z.B. Zhan, L.B. Di, X.L. Zhang, Catal. Today 256 (2015) 148.

[25] X. Liang, C.J. Liu, P. Kuai, Green Chem. 10 (2008) 1318.

[26] L.B. Di, X.L. Zhang, Z.J. Xu, K. Wang, Plasma Chem. Plasma P. 34 (2014) 301.

[27] J.P. Hong, J. Du, B. Wang, Y.H. Zhang, C.C. Liu, H.F. Xiong, F.L. Sun, S.F. Chen, J.L. Li, ACS Catal. 8 (2018) 6177.

[28] B. Qi, L.B. Di, W.J. Xu, X.L. Zhang, J. Mater. Chem. A 2 (2014) 11885.

[29] L.B. Di, Z.J. Xu, K. Wang, X.L. Zhang, Catal. Today 211 (2013) 109.

[30] Z. Li, X.L. Zhang, Y.Z. Zhang, D.Z. Duan, L.B. Di, Plasma Sci. Technol. 20 (2018) 014016.

[31] Y.Z. Li, Y. Yu, J.G. Wang, J. Song, Q. Li, M.D. Dong, C.J. Liu, Appl. Catal. B 125 (2012) 189.

[32] M. Kruk, M. Jaroniec, Chem. Mater. 13 (2001) 3169.

[33] L.H. Qu, C.Q. He, Y. Yang, Y. L. He, Z.M. Liu, Mater. Lett. 59 (2005) 4034.

[34] Z.Y. Li, S.L. Ren, J. Mater. Sci. 50 (2015) 4600.

[35] J. Lian, X. Fang, W. Liu, Q. Huang, Q. Sun, H. Wang, H. Wang, X. Wang, W. Zhou, Top. Catal. 60 (2017) 831.

[36] W. Chu, J. Xu, J. Hong, T. Lin, A. Khodakov, Catal. Today 256 (2015) 41.

[37] E. C. Neyts, K. Ostrikov, M. K. Sunkara, A. Bogaerts. Chem. Rev. 115 (2015) 13408.[38] C.Q. Hu, J.K. Pulleri, S.W. Ting, K.Y. Chan, Int. J. Hydrogen Energ. 39 (2014) 381.

Table captions

Table 1. The sizes of Pd nanoparticles (D_{Pd}), the composition of Pd species, and the Pd/C atomic ratios for the Pd/C catalysts before and after 3 reaction cycles.

Table 2. BET and ICP-OES results of the Pd/C catalysts.

Table 1

Sample	D_{Pd} (nm)	Pd composition (%)			Atomic ratios of Pd/C
		Pd^0	Pd^{II}	Pd^{IV}	
Pd/C-P	2.7±1.1	66.0	21.8	12.2	0.0140
Pd/C-P-3R	2.7±0.9	53.1	24.7	22.2	0.0125
Pd/C	3.3±1.1	55.4	33.4	11.2	0.0147
Pd/C-3R	4.0±1.1	54.6	31.3	14.1	0.0087

Table 2

Sample	V_p ($cm^3 \cdot g^{-1}$)	D_p (nm)	S_{BET} ($m^2 \cdot g^{-1}$)	Pd (wt%)
Pd/C	0.444	3.82	913.7	5.10%
Pd/C-R	0.358	3.83	707.5	4.86%
Pd/C-3R	0.270	3.80	635.5	4.48%
Pd/C-P	0.007	3.80	822.2	5.02%
Pd/C-P-R	0.005	3.81	653.2	4.88%
Pd/C-P-3R	0.017	3.81	620.1	4.65%

Figure captions (only color on the web):

Fig. 1. Catalytic activity of Pd/C-P and commercial Pd/C for HCOOH dehydrogenation.

Fig. 2. Catalytic stability of Pd/C-P and commercial Pd/C for HCOOH dehydrogenation.

Fig. 3. XRD patterns of Pd/C-P and commercial Pd/C before and after HCOOH dehydrogenation reaction.

Fig. 4. Typical TEM images of (a) Pd/C-P, (b) Pd/C, (c) Pd/C-P-3R, and (d) Pd/C-3R, as well as the corresponding histograms of size distribution of Pd nanoparticles.

Fig. 5. XPS spectra of Pd3d in Pd/C-P, Pd/C-P-3R, Pd/C and Pd/C-3R.

Fig. 6. (a,b) Nitrogen adsorption-desorption isotherms of Pd/C-P, Pd/C-P-3R, Pd/C and Pd/C-3R, and (c,d) the corresponding pore size distribution curves.

Fig. 1

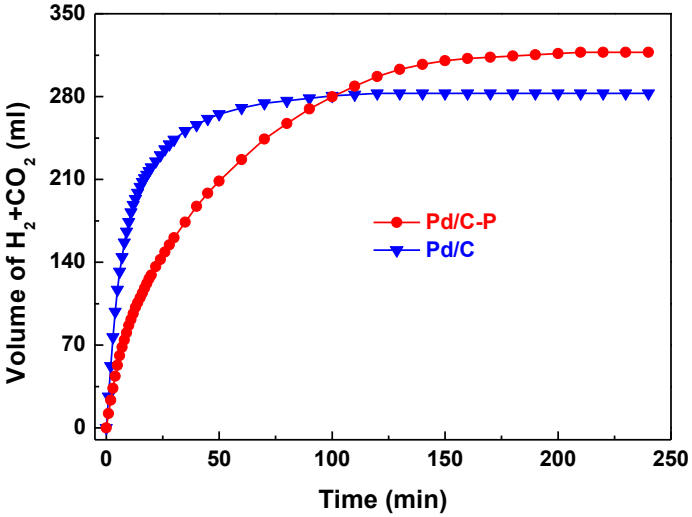
Volume of H_2+CO_2 (ml)
Time (min)
Pd/C-P
Pd/C
0
70
140
210
280
350
0
50
100
150
200
250

Fig. 2

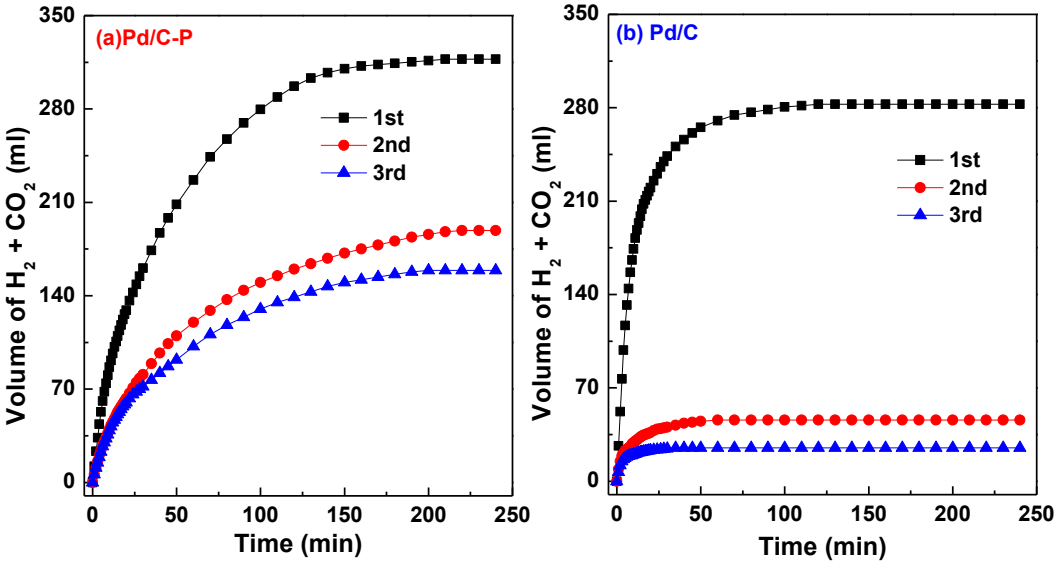
(a)Pd/C-P
(b) Pd/C
Volume of H_2 + CO_2 (ml)
Time (min)
1st
2nd
3rd
0
70
140
210
280
350
0
50
100
150
200
250

Fig. 3

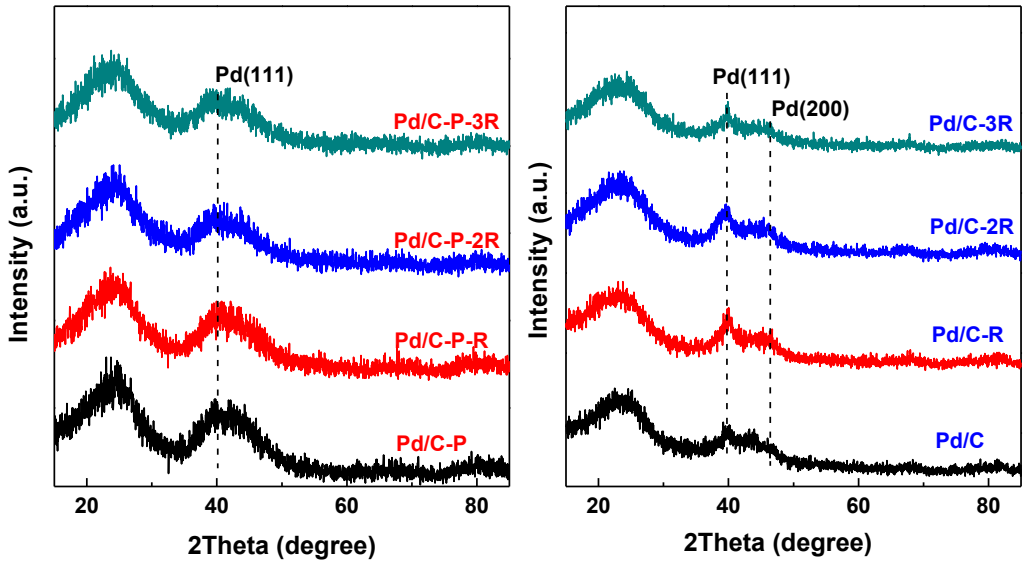
Pd(111)
Pd/C-P-3R
Pd/C-P-2R
Pd/C-P-R
Pd/C-P
Intensity (a.u.)
20
40
60
80
2Theta (degree)
Pd(111)
Pd(200)
Pd/C-3R
Pd/C-2R
Pd/C-R
Pd/C
Intensity (a.u.)
20
40
60
80
2Theta (degree)

Fig. 4

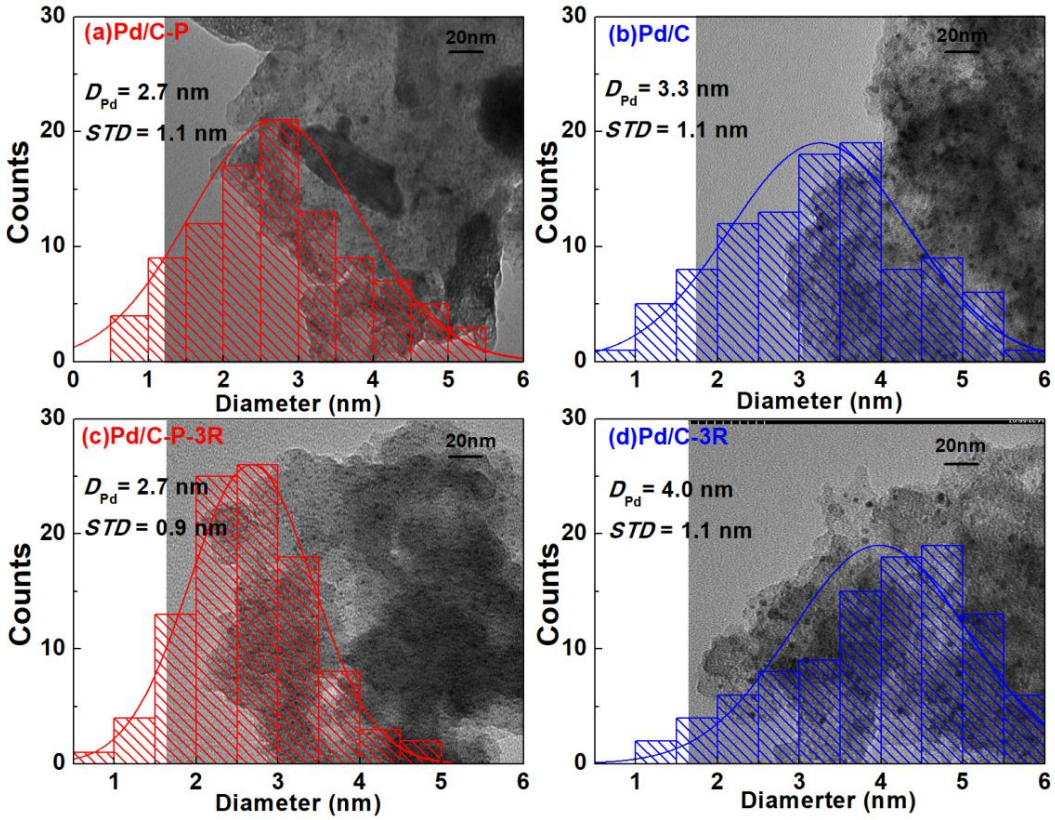
(a)Pd/C-P
20nm
D_{Pd} = 2.7 nm
STD = 1.1 nm
Counts
Diameter (nm)
(b)Pd/C
20nm
D_{Pd} = 3.3 nm
STD = 1.1 nm
Counts
Diameter (nm)
(c)Pd/C-P-3R
20nm
D_{Pd} = 2.7 nm
STD = 0.9 nm
Counts
Diameter (nm)
(d)Pd/C-3R
20nm
D_{Pd} = 4.0 nm
STD = 1.1 nm
Counts
Diamerter (nm)

Fig. 5

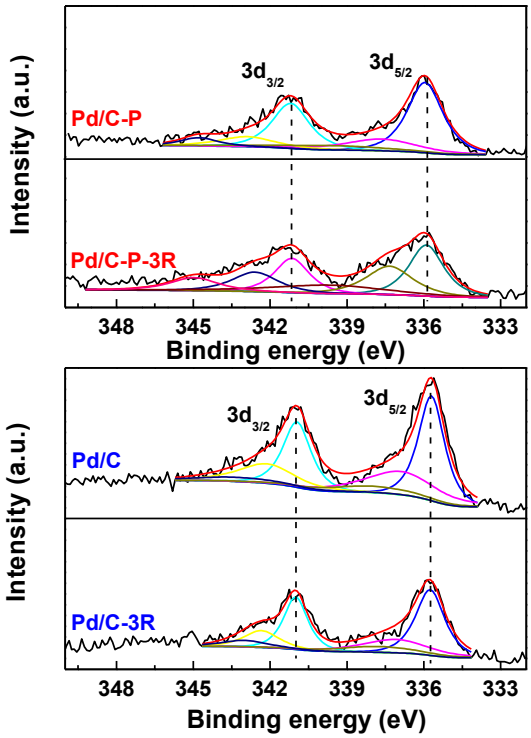
Intensity (a.u.)
3d3/2
3d5/2
Pd/C-P
Pd/C-P-3R
348
345
342
339
336
333
Binding energy (eV)
Intensity (a.u.)
3d3/2
3d5/2
Pd/C
Pd/C-3R
348
345
342
339
336
333
Binding energy (eV)

Fig. 6

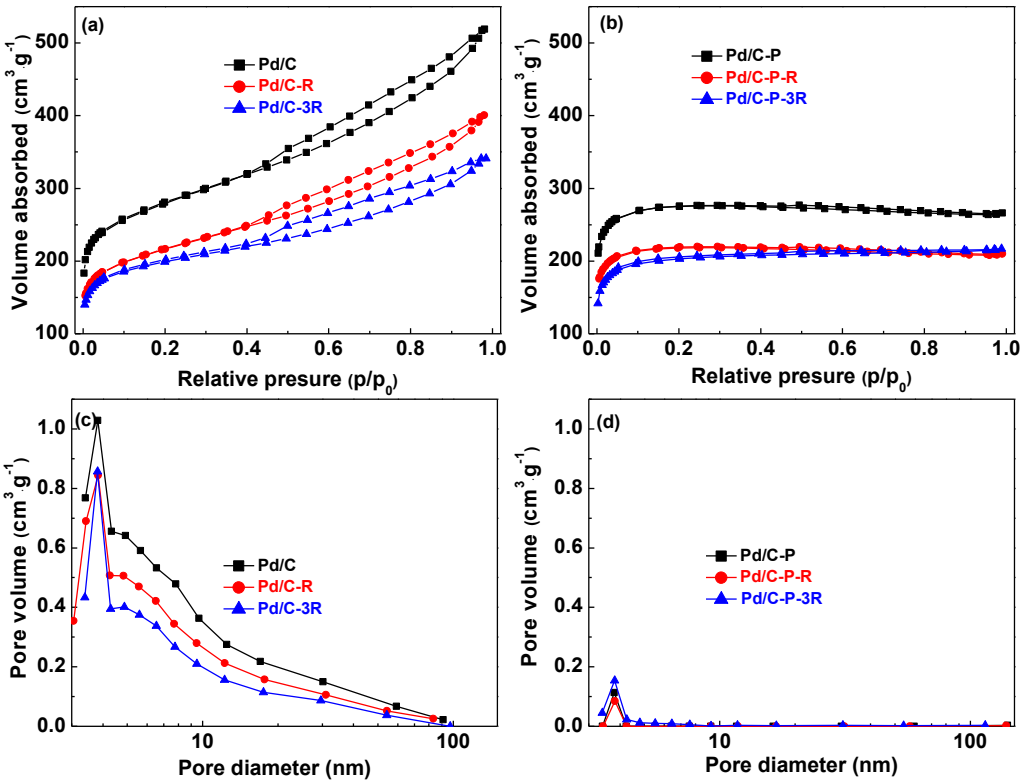
(a)
Pd/C
Pd/C-R
Pd/C-3R
Volume absorbed (cm3 g-1)
Relative presure (p/p0)
(b)
Pd/C-P
Pd/C-P-R
Pd/C-P-3R
Volume absorbed (cm3 g-1)
Relative presure (p/p0)
(c)
Pd/C
Pd/C-R
Pd/C-3R
Pore volume (cm3 g-1)
Pore diameter (nm)
(d)
Pd/C-P
Pd/C-P-R
Pd/C-P-3R
Pore volume (cm3 g-1)
Pore diameter (nm)